Annals of Biomedical Engineering, Vol. 42, No. 7, July 2014 *(© 2013)* pp. 1508–1516
DOI: 10.1007/s10439-013-0933-0

Porous Implants Modulate Healing and Induce Shifts in Local Macrophage Polarization in the Foreign Body Reaction

ERIC M. SUSSMAN,[1] MICHELLE C. HALPIN,[1] JEANOT MUSTER,[2,4,5] RANDALL T. MOON,[2,4,5] and BUDDY D. RATNER[1,3,5]

[1]Department of Bioengineering, University of Washington, Box 355061, William H. Foege Building, Room N330J, Seattle, WA, USA; [2]Department of Pharmacology, University of Washington, Seattle, WA, USA; [3]Department of Chemical Engineering, University of Washington, Seattle, WA, USA; [4]Howard Hughes Medical Institute, University of Washington School of Medicine, Seattle, WA, USA; and [5]Institute for Stem Cell and Regenerative Medicine, University of Washington School of Medicine, Box 358056, 850 Republican Street, S525, Seattle, WA, USA

(Received 2 July 2013; accepted 29 October 2013; published online 19 November 2013)

Associate Editor Tzung Hsiai oversaw the review of this article.

Abstract—The foreign body reaction (FBR) to implanted materials is of critical importance when medical devices require biological integration and vascularization to support their proper function (e.g., transcutaneous devices, implanted drug delivery systems, tissue replacements, and sensors). One class of materials that improves FBR outcomes is made by sphere-templating, resulting in porous structures with uniform, interconnected 34 μm pores. With these materials we observe reduced fibrosis and increased vascularization. We hypothesized that improved healing is a result of a shift in macrophage polarization, often measured as the ratio of M1 pro-inflammatory cells to M2 pro-healing cells. In this study, macrophage polarity of 34 μm porous implants was compared to non-porous and 160 μm porous implants in subcutaneous mouse tissue. Immunohistochemistry revealed that macrophages in implant pores displayed a shift towards an M1 phenotype compared to externalized cells. Macrophages in 34 μm porous implants had up to 63% greater expression of M1 markers and up to 85% reduction in M2 marker expression ($p < 0.05$). Macrophages immediately outside the porous structure, in contrast, showed a significant enrichment in M2 phenotypic cells. This study supports a role for macrophage polarization in driving the FBR to implanted materials.

Keywords—M1, M2, Vascularization, Foreign body capsule, Sphere-templated porous scaffolds.

INTRODUCTION

The foreign body reaction (FBR) is the biological response to implanted materials.[5,25,55] It is characterized by a sequence of events that begin when the implantation takes place. These events include the recruitment of multiple cell types including macrophages, fibroblasts, myofibroblasts, and others that are involved in a complex process resulting in encapsulation of the implant with a collagenous avascular "scar" known as the foreign body capsule (FBC). The FBC can negatively impact the function of medical devices, by inhibiting integration, reducing blood supply, causing contraction and pain, and blocking long-term drug release. Thus, much effort has focused on developing a better understanding of the FBR so that therapies can be designed to eliminate it.

Many have speculated that the presence and type of macrophage has a key role in coordinating the FBR.[55] Indeed, in the absence of macrophages the histological hallmarks of the FBR are absent.[35] Macrophages are present at the implant site in large numbers within days and some will reside at the implant surface for the life of the implant. The macrophage attempts to phagocytose foreign materials and is also known to release a multitude of signaling molecules including growth factors, cytokines, and chemokines that impact the behavior of other cells. The cumulative effect of the macrophage's influence is thought to determine the long-term outcome of the FBR. Many studies have been performed to understand the relationship between device design and macrophage activation.[15,39,46,51] The goal of those studies was generally to reduce the number of macrophages or degree of inflammatory marker expression within those cells. However, such research, though providing useful insights into the FBR, has for the most part not led to

Address correspondence to Buddy D. Ratner, Department of Bioengineering, University of Washington, Box 355061, William H. Foege Building, Room N330J, Seattle, WA, USA. Electronic mail: ratner@uweb.engr.washington.edu

the development of principles that guide device design through altering macrophage behavior.

Macrophages are activated while they are participating in local tissue responses including the FBR, wound healing, and certain diseases. Activation characteristics are not uniform, however, and therefore they have been categorized according to a scale known as macrophage polarization.[30,36] M1-polarized macrophages are generated *in vitro* using lipopolysaccharides and interferon-gamma (IFN-gamma) and are considered a pro-inflammatory phenotype.[30] M1 macrophages are commonly detected *in vivo* using markers including inducible nitric oxide synthase (iNOS/NOS2)[33] and interleukin-1 receptor 1 (IL-1R1),[30] among others. M2-polarized macrophages are typically generated *in vitro* using IL-4 or IL-13 and are considered a pro-healing phenotype. M2 macrophages are commonly detected *in vivo* using the markers macrophage mannose receptor (MMR)[45] and scavenger receptor B I/II (SR-B1/II),[30,31] among others.

In multiple disease models, it has been shown that the polarity of macrophages influences the severity of the disease.[6,22,48,56] The specific macrophage polarization needed to improve health is disease-dependent. For example, in injured spinal cord M1 macrophages may cause neurotoxicity,[22] while in cancer M2 macrophages may favor tumor progression.[44] Significant research effort has also focused on understanding the nature of the innate immune response in the FBR.[4,8,15,24,41] However, there is still only limited evidence to suggest that improved healing can be achieved through a shift in macrophage behavior (Mokarram *et al.*[34] and Badylak *et al.*[6] for example).

In the present study, we describe the quantification of macrophage polarity at the sites of subcutaneously-implanted hydrogels with well-defined porosity in mice. These hydrogels are engineered through their porosity (or lack thereof) to elicit different FBRs, and we provide evidence that improved FBRs (less fibrosis, more vascularization) are associated with an implant-localized macrophage polarization shift from M2 to M1.

MATERIALS AND METHODS

Implant Material Preparation

Sphere-templated pHEMA scaffolds for implantation with nominal pore sizes of 34 or 160 μm $\pm$ 12% were prepared using previously-published techniques.[38] Poly(methyl methacrylate) (PMMA) beads were obtained from Microbeads AS (Skedsmokorset, Norway, 34 μm) and Polysciences, Inc. (Warrington, PA, 160 μm) and sorted using an ATM Sonic Sifter (Milwaukee, WI) to obtain a particle size distribution reflecting the sieve mesh size required for each range. These sifted beads were poured into a 75 $\times$ 25 $\times$ 1 mm^3 rectangular mold comprised of glass slides separated by a spacer and held together with metal binder clips. Filled molds were placed inside a glass beaker and sonicated for 30 min in a water bath to close-pack the spherical beads, then sintered at 140 °C for 26 h (160 μm) or 177 °C for 28 h (34 μm) to obtain fused bead cakes in which the diameter of the fusion interfaces were 30% of the bead diameter. The interstices of these bead cakes were then filled with pHEMA precursor solutions and polymerized under broad-spectrum UV light from a high-intensity mercury lamp. Non-porous scaffolds were fabricated by pouring the HEMA monomer solution precursor into molds without PMMA beads. The HEMA monomer solution consisted of 5 mL ophthalmic grade 2-hydroxyethyl methacrylate (Polysciences), 0.23 mL tetraethyleneglycoldimethacrylate (Polysciences), 2.0 mL deionized water. 1.5 mL ethylene glycol, and 76 mg Irgacure 651 (BASF, Freeport, LA). After UV polymerization, the scaffolds were removed from the mold and scraped with a razor blade to remove the non-porous surrounding skin that is sometimes noted. Soxhlet extraction was next performed in dichloromethane and then acetone for 24 h each in order to remove the PMMA. Scaffolds were cut to 3 mm discs using biopsy punches and placed in 70% ethanol (3 $\times$ 1 h) for sterilization. Ethanol was slowly exchanged for sterile PBS and samples were stored at 4 °C until implantation. Scanning electron microscopy was performed on lyophilized samples to confirm that the dimensions of the scaffolds adhered to specifications.

Cytotoxicity and Endotoxin Testing

Samples from each batch were removed for cytotoxicity and endotoxin testing. Cytotoxicity testing was performed according to ISO standards 10993-5 and 10993-12. Scaffolds were extracted for 24 h in DMEM culture media followed by exposing live 3T3 cells to this conditioned media for 48 h. Visual microscopic inspection and grading did not reveal a cytotoxic response due to material extracts compared to controls. Endotoxin testing was performed according to the manufacturer's protocol (Lonza). Three scaffolds from each batch were extracted into 500 μL endotoxin-free water. All scaffold extracts were negative for endotoxin ($<$0.6 EU/mL).

Surgical Procedure

All animal experiments adhered to federal guidelines and were approved by the University of Washington Animal Care and Use Committee. Mouse

implantations were performed in seven to nine-month old BAT-gal mice, a transgenic reporter line for WNT signaling built on the B6D2F1 background. Mice were anesthetized with a ketamine/xylazine cocktail. The backs were shaved and sterilized and a midline incision was made. Subcutaneous pockets were formed on both sides of the incision down to the underside of the mice. On each side, one implant was placed with a total of 10 implants of each type (non-porous, 34 and 160 μm) implanted into 15 mice. The incision was closed with surgical staples and mice were monitored during recovery until fully active.

Explant Procedure

Explantation was performed 21 days after implantation. Mice were euthanized by asphyxiation with carbon dioxide. Two midline incisions were made parallel to the original incision on both sides. The incision was performed through the muscle layer and continued forward and backwards down to the base of the limbs, allowing the entire side wall to be exposed. The implant was located and dissected out. Samples were fixed in zinc fixative for 2 h followed by storage in 70% ethanol and paraffin wax embedding. Slides were prepared from paraffin blocks cut with 5 μm sections.

FBC Thickness Measurement

Masson's trichrome staining was performed on tissue sections from all explants. We observed that a substantial number of explants were encased in large amounts of adipose tissue, and that the presence of this fat correlated with obvious reductions in cell infiltration and collagen deposition. It was therefore necessary to eliminate variability in the results by choosing to analyze implants with minimal to zero adipose encasement. This resulted in a final sample set of three explanted scaffolds of each pore size. Sudan-black stained sections were used to assess capsule thickness. A minimum of six high magnification fields per implant were employed and a rectangular region was drawn over the capsule using ImageJ image analysis software (National Institute of Health, USA). The areas of these regions were divided by their lengths to obtain the average thickness per image, and the thicknesses were averaged for each explant.

Vessel Density Measurements

Immunohistochemistry was performed for the endothelial cell marker CD31 (BD Pharmingen) in order to visualize blood vessels in explanted tissue. Alexa Fluor Donkey anti-rat 594 was used as the secondary detection agent and sections were counterstained with DAPI and 0.3% sudan black. Images were collected using a Nikon TE-200 inverted microscope. A blinded observer then counted the number of vessel profiles within each of two regions of each image: 68 μm outside of the scaffold from its edge, and 68 μm inside of the scaffold from its edge. From here on, these regions will be referred to as "inside" and "outside" the scaffold. They were chosen based on being the thickness of two full pores of a 34 μm porous scaffold and are of a scale on par with cellular integration and FBC thicknesses. The total number of vessels for each implant region were added and divided by the total area of tissue analyzed. The data is reported as average number of blood vessel profiles per square mm per implant type.

Fluorescence Immunohistochemistry for Macrophage Markers

Standard methods were used for performing fluorescence immunohistochemistry on sections of explant tissue. Antigen retrieval was conducted as necessary by placing slides in microwave-boiled pH 6.0 citrate buffer and allowing them to cool to room temperature (RT). Blocking solutions consisted of 5% normal donkey serum (Jackson ImmunoResearch Laboratories, Inc., West Grove, PA), 1% IHC-grade bovine serum albumin (Vector Laboratories, Inc., Burlingame, CA), and 0.05% Tween-20 in pH 7.6 Tris-buffered saline. Blocking solution was applied for 30 min at RT and all further antibody incubations were performed in blocking solution. Primary antibodies rat anti-F4/80 clone BM8 (BMA Biomedicals, Augst, Switzerland), rabbit anti-nitric oxide synthase 2 (NOS2), rabbit anti-interleukin 1 receptor 1 (IL-1R1), rabbit anti-scavenger receptor B I/II (SRBI/II) (Thermo Fisher Scientific Inc., Rockford, IL), and goat anti-MMR (R&D Systems, Minneapolis, MN) were applied overnight at 4 °C. For negative controls, isotype-matched IgG was applied to control sections at the same concentration as the corresponding primary antibody. These sections did not reveal staining.

The secondary antibody cocktail consisted of Alexa Fluor 350 donkey anti-goat (1:100, Invitrogen), Alexa Fluor 488 donkey anti-rabbit (1:200, Invitrogen), and Alexa Fluor 594 donkey anti-rat, incubated at RT for 1 h. For each implant, at least five fields containing macrophages were imaged at 40×. Only macrophages (F4/80+) located within 68 μm of the edge of the implanted scaffolds were included in the count. Cells were categorized according to the presence of the marker being studied and the average percentage of each macrophage type was determined.

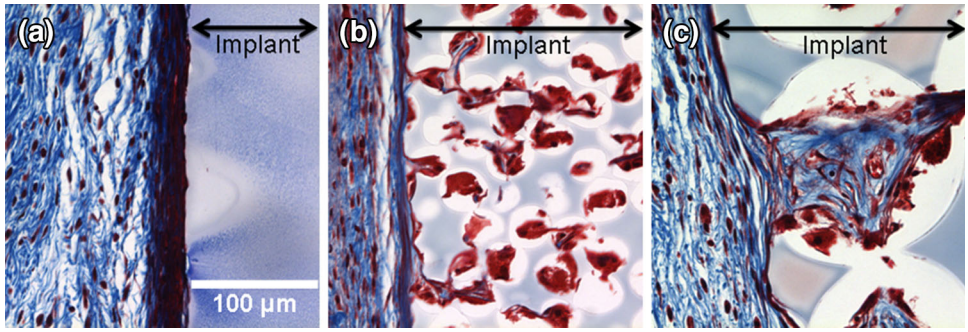

FIGURE 1. The cellular and collagen composition of the foreign body reaction to solid and porous implants is pore-size dependent. Representative Masson's trichrome photomicrographs show histological responses based on pore size. Collagen is shown in blue, cellular cytoplasm in red, and cell nuclei in black. (a) Non-porous implants have a dense FBC at the implant edge, (b) 34 μm porous scaffolds have a highly cellular infiltrate, and (c) 160 μm porous scaffolds have a cellular infiltrate that is much richer in collagen than in 34 μm scaffolds.

Statistics

At least six high-powered fields were analyzed per implant per marker of interest. The cell counts for all images of a particular implant were added and then divided by the total area measured across the images. The measurements were then averaged across implants of like pore size. All averages are described along with the 95% confidence interval of the measurement based on a normal data distribution.

RESULTS

The differences in the FBRs for non-porous, 34 μm porous, and 160 μm porous implants were clearly evident. Thus, we could relate FBRs with different histological features to measured macrophage phenotypes. Inspection of Masson's trichrome-stained sections reveals easily-distinguished pore structure-specific morphological features of tissue within pores and within the surrounding FBC (Fig. 1). Non-porous implants (Fig. 1a) undergo a prototypical FBR, consisting of a fibrous collagen capsule aligned with the implant surface and containing a heavy cell infiltrate, especially at the implant surface. The 34 μm pore implants (Fig. 1b) are also surrounded by a fibrous capsule, though thinner and less dense than the capsule surrounding the non-porous implant and with the additional feature that the pores are infiltrated with a mostly cellular and slightly fibrous tissue substance. Finally, the 160 μm pore materials (Fig. 1c) are visibly distinguished from the 34 μm porous materials because the pores contain a greater fraction of fibrous tissue. Neither the 34 nor 160 μm pore materials had as large a cell infiltrate at the implant interfaces as the non-porous implants. Thus, each implant type elicited a unique tissue response, and it was the goal of this study to explore the mechanism for those observed differences.

Analysis of CD31-stained sections of implant tissue was used to quantify differences in vascularization of the three scaffold types (Fig. 2a). A statistically significant increase ($p < 0.05$) in the blood vessel density is observed inside 34 μm pore scaffolds (90 ± 19 vessels/mm^2) vs. 160 μm pore scaffolds (51 ± 10 vessels/mm^2). A similar trend is observed in tissue adjacent to implanted scaffolds, however without statistical significance. Thus, improved vascularization is observed for 34 μm pore scaffolds compared to the other scaffold morphologies tested.

FBC thickness measurements were performed to make additional quantitative comparisons of healing based on pore size. The average thicknesses of the FBCs surrounding implants are 43 ± 19, 62 ± 16, and 87 ± 44 μm, for non-porous, 34 μm pore and 160 μm pore materials, respectively. It is noted that although a statistical difference is not found between these measurements ($p > 0.05$), that the upper limit of the confidence interval for 160 μm pore implants is much greater than the other two implant types. Based on the intensity of the trichrome stain blue color, the capsule surrounding the solid implant would appear to be comprised of higher density (more fibrous) collagen compared to the two porous specimens. Additionally, reduced fibrosis is observed at the implant interface and inside the pores of 34 μm pore scaffolds (Fig. 1), indicating improved healing.

Macrophage density was examined as an explanation for histological differences observed. The total number of macrophages was counted and is shown in Fig. 2b. There is no statistical difference in macrophage density in pores or in the FBC based on implant type. Thus, macrophage density does not provide a direct explanation for histological differences.

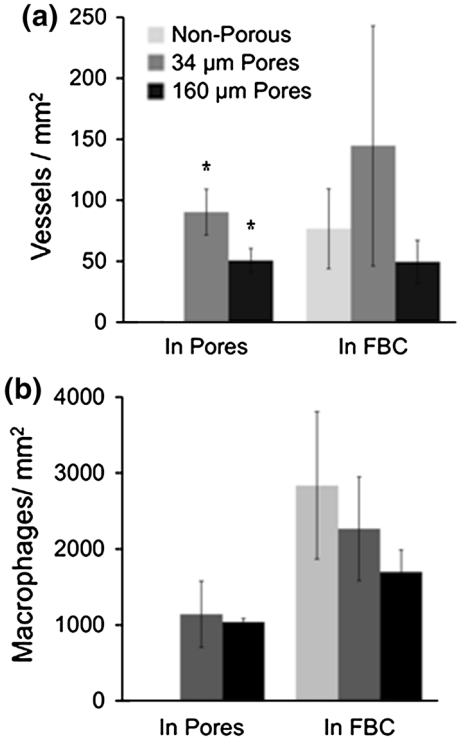

FIGURE 2. Implants with 34 μm pores elicit greater numbers of blood vessels but have the same number of macrophages as non-porous and 160 μm porous implants. (a) A statistically significant increase blood vessel density is observed inside pores (* $p < 0.05$), while in the FBC the same trend is also observed but not statistical ($p > 0.05$). (b) No statistically significant difference in macrophage density is observed when comparing implant types either in pores or in the FBC ($p > 0.05$).

Since macrophage density did not correlate with histological differences caused by pore morphology, macrophage polarization was next examined using fluorescence immunohistochemistry to determine if cell phenotype could be tied to the healing response (Fig. 3). Cells were stained with three markers: DAPI for nuclei, F4/80 for macrophage identification, and one of four M1 and M2 polarization markers. In general, expression of M1 markers NOS-2 and IL-1R1 is observed inside scaffold pores (Figs. 3e, 3f, 3i, and 3j) and on scaffold outer surfaces (Figs. 3a and 3b). Conversely, expression of M2 markers MMR and SR-BI/II is generally observed in the FBC (Figs. 3c–3e, 3h, 3k, and 3l) and in the central region of 160 μm pores (Figs. 3k and 3l). This location-specific marker expression is most apparent for 34 μm pore implants (Figs. 3e and 3g, for example), in which the pores are filled with a nearly-exclusive population of M1+M2− cells,

The quantification of polarity marker expression is presented in Fig. 4. To ensure that only macrophages would be considered, all cells counted as either M1+ or M2+ were double positive for F4/80. M1 expression is up to 63% greater in pores compared to in FBC. NOS2+ percentages increase from 18 ± 5 to 81 ± 2% and from 24 ± 9 to 64 ± 15% for 34 and 160 μm porous scaffolds, respectively, when comparing the implant pores to the FBC ($p < 0.05$ for both). Similarly, IL-1R1+ percentages increase from 42 ± 4 to 86 ± 13% and from 50 ± 6 to 81 ± 3% for 34 and 160 μm porous scaffolds ($p < 0.05$ for both). No statistical differences are observed for M1+ percentages outside non-porous implants compared to porous implants ($p > 0.05$), indicating that M1 expression in the FBC is not greatly influenced by the adjacent implant pore structure.

M2 expression is up to 85% less in pores compared to in FBC. MMR+ percentages decrease from 88 ± 1 to 3 ± 5% and from 85 ± 12 to 44 ± 9% for 34 and 160 μm porous scaffolds, respectively, when comparing implant pores to the FBC ($p < 0.05$ for both). SR-BI/II+ percentages decrease from 50 ± 7 to 21 ± 2% ($p < 0.05$) and increase from 36 ± 9 to 42 ± 15% ($p > 0.05$) for 34 and 160 μm porous scaffolds. M2+ percentages appear lower ($p < 0.05$ for MMR but not for SR-BI/II) in the FBC surrounding non-porous implants compared to porous implants, indicating that pores do have the ability to influence M2 expression in the adjacent FBC.

Finally, the major findings of this study are summarized in Fig. 4c, in which the ratio of polarity markers are compared between the FBC and within scaffold pores. As indicated above, macrophage polarization was greatest (highest and lowest fold differences when comparing implant pores to FBC) for 34 μm pore implants. The trends were similar, however not as large in the 160 μm pore implants.

DISCUSSION

The present study is a comparison of the FBR to hydrogel scaffolds of differently defined pore structures. In a previous report,[28] we showed that sphere templated materials with a pore diameter of about 34 μm and with interconnected pore throats of about 29% enhance angiogenesis and reduce fibrosis at muscular implant sites. Here we sought to compare these 34 μm pore optimized materials to larger, non-optimal 160 μm pore and standard non-porous materials in search of a mechanism for the pro-healing effects of 34 μm pores. In the present study, the vascular density of subcutaneously-implanted scaffolds was significantly greater in 34 μm pores compared to 160 μm pores (Fig. 2a), thus supporting the previous findings and demonstrating the pro-healing effect in subcutaneous tissue. Since macrophage infiltrates were largely similar in number between scaffold types (Fig. 2b), we turned to differences in macrophage

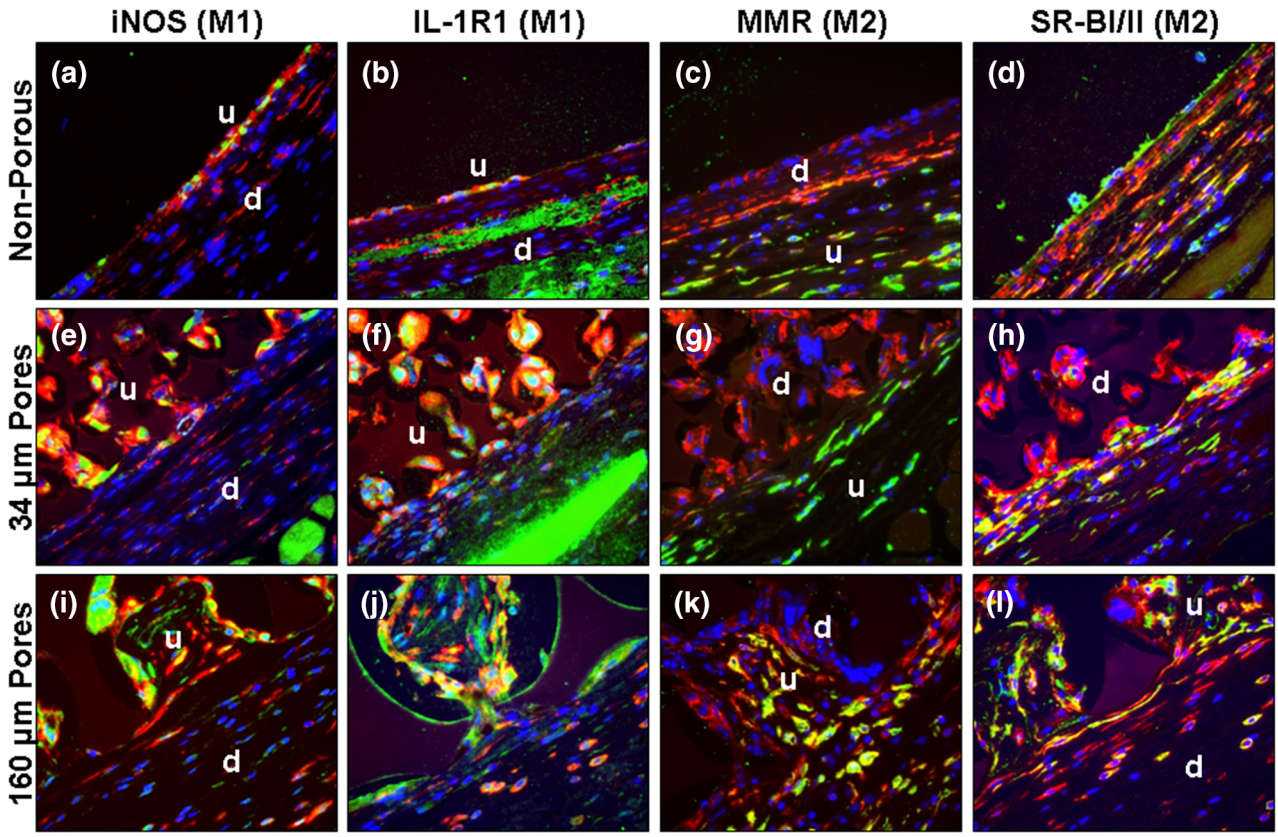

FIGURE 3. Distinct, location-specific macrophage populations in the FBR are visualized using M1 and M2 markers. Images are of the implant–FBC interface with the implant in the upper-left and adjacent tissue in the lower-right. Colors are blue = nuclei (DAPI), red = macrophages (F4/80), and green = polarity marker (varies). M1 markers are iNOS (a, e, i) and IL-1R1 (b, f, j) and M2 markers are MMR (c, g, k) and SR-BI/II (d, h, l). Images are representative of the response to non-porous (a–d), 34 μm porous (e–h), and 160 μm porous 3-week implants (i–l). Up-regulation (u) and down-regulation (d) of the polarity marker under examination within a particular frame are indicated. Particularly noteworthy is high M1 marker expression in 34 μm pores (e) and low in adjacent FBC, and *vice versa* for M2 markers (g).

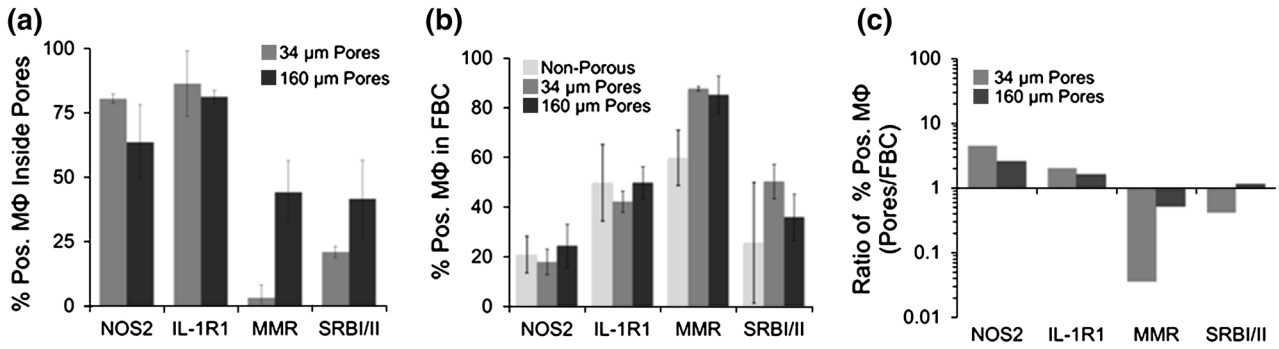

FIGURE 4. Macrophage localization to pores promotes M1 marker expression while macrophage localization to FBC promotes M2 marker expression. (a) M1 marker expression is high (>50%) and M2 marker expression is low (<50%) inside porous implants, and this observation is exaggerated 34 μm implants compared to 160 μm porous implants. (b) In the FBC, a reduction in M1 marker expression and increase in M2 marker expression is observed, with little observed correlation with the pore size of the material. (c) The ratio of marker expression inside pores to within the FBC is >1 for M1 markers and generally <1 for M2 markers, with an increase in this trend observed for 34 μm porous implants.

phenotype (polarization) as the driving force for enhanced healing.

Distinctive macrophage polarization patterns were observed based on implant type and macrophage localization—the percentage of M1+ macrophages was enhanced in the pores and on the outer surfaces of implants compared to within the FBC. This observation agrees with previous work,[29,47] in which macrophages

adherent to implanted materials displayed increased inflammatory characteristics compared to their neighbors in the FBC. In fact, numerous previous studies have shown that cells in the FBR produce markers consistent with M1 activation[8,41,42,52]; however few have delineated the specific location of these cells as we do here.

M2+ macrophages were found in areas distinct from M1+ macrophages, namely away from implant surfaces and in the FBC. Finding these markers indicative of pro-healing M2 macrophages was not unexpected given that previous studies have demonstrated active IL-4 in implant exudate[18,20] and IL-4 is a typical cytokine used to elicit M2-polarized macrophages *in vitro* and *in vivo*.[34] M2+ macrophages were nearly eliminated within 34 μm pore scaffolds but only somewhat reduced within the pores of 160 μm implants. Cell interaction directly with the scaffold pore walls appeared to be the greatest inhibitor of M2 markers, as M2+ cells resided in close quarters, encircled by M2− cells within the large 160 μm pores (Fig. 3k). At the surface of non-porous implants, a noticeably thick layer of M2− cells was present (Fig. 3c). These observations suggest that M2 down-regulation is determined by adhesion to surfaces and pore walls, since M2+ and M2− are otherwise observed adjacent to each other. At this 3-week time point, the default polarity for a macrophage in the FBR appears to be M2+, unless it is adherent to the surface of the implant pores.

Consideration for co-expression of M1 and M2 markers must also be made. While M1 and M2 cells are often thought to be different phenotypes, simultaneous M1 and M2 marker expression might occur due to the local milieu and has been previously reported.[6,28] In fact, based on the population percentages we report above, many macrophages in the FBR are M1+M2+. Significantly, the area in which we observed the greatest polarization (almost exclusively M1+M2−) was within 34 μm pores, stimulating new ideas about a mechanism for enhanced vascularization and reduced fibrosis of those scaffolds. Interestingly, while the M1 phenotype is most often associated with increased fibrosis,[40] there are suggestions that M2 macrophages can lead to fibrosis and that there may even be a specific fibrotic phenotype of the macrophage.[2]

Two distinct populations of activated macrophages are identified in the FBR. We observed a strong increase in M1+ cells proximal to the implant and a strong decrease in M2+ cells directly adherent to the implant. Many studies have attempted to correlate macrophage polarization with FBR outcome.[8,17,19,26,32,41,42,52] In particular, work by Badylak and coworkers[6,9] has demonstrated a correlation between M2 macrophages and improved integration of implanted biological scaffolds. The present study suggests that M1+M2− cells are not necessarily associated with a decrease in implant integration and vascularization. One major difference between the two studies is the use of biological scaffolds vs. synthetic ones here. We did notice a large M2+ cell population in the FBC. It is possible that under conditions of poor biocompatibility, the polarization of macrophages in the FBC could be shifted, although that was predominantly not observed here. Further work is required to understand specifically how cell phenotype might influence implant healing outcomes.

Porous materials for implants have been of significant historical interest due to their ability to integrate with surrounding tissue and heal with reduced FBRs.[23,50] Numerous accounts describe thinner FBCs and increased vascularization of porous materials.[10,53] In studies in which the effect of pore size is investigated, pore sizes in the range of 34 μm often are shown to increase vascularization and reduce FBC.[7,43] This study reveals that the mechanism behind which porous materials have improved healing might involve a shift in the polarity of macrophages at the implant site. Other researchers have reported decreases in M1 and increases in M2 gene expression in the FBR with time.[14,16,41] Such plasticity in macrophage phenotype is found in other disease models as well.[37] The role of pore-bound macrophages may be to alter the timeline of cytokine expression in the FBR and tip the balance towards better healing.

This study was performed at 3 weeks post-implantation and thus only provides a snapshot of the FBR. It is well known that the FBR is a dynamic series of events,[3] and macrophage polarization earlier and later in the FBR may play an important role. Future studies of the time course of macrophage polarity in response to porous implants are suggested.

Many studies explore the role of macrophage phenotype in inflammation-associated conditions such as injury, cancer, and auto-inflammatory disease.[11,22,49,56] While M1 and M2 polarizations have generally been classified as pro-inflammatory and pro-healing, respectively, exceptions exist.[56] For example, pore-bound M1 macrophages, being pro-inflammatory, are not expected to support significant fibrosis.[54] Further, M2 macrophages, close to pores but without a thick cellular barrier seen on non-porous implants, could release, and transport pro-angiogenic cytokines.[21]

In this study, cells were classified according to their expression of markers thought to be indicative of macrophage phenotype. IL-1R1, MMR, and SR-BI/II are plasma membrane-bound receptor proteins and iNOS is a cytoplasmic protein responsible for nitric oxide production.[1,12,13,27] It is recognized that the

detection of these markers does not imply the overall behavior of the cells including growth factor, cytokine and chemokine expression, and reactive oxygen species release. These specific behaviors are what are thought to ultimately coordinate the FBR. Simplified, we have further distinguished the phenotype between pore-adherent and non-adherent macrophages. For 34 μm porous implants, there is little available space for a macrophage to reside without touching a pore surface. Clearly, porous materials increase the size of the adherent macrophage population and that could be the cause of improved healing. Further work to identify the functional differences of adherent- and non-adherent macrophages is needed to elucidate the role of polarization in improved healing.

ACKNOWLEDGMENTS

These studies were funded by University of Washington Engineered Biomaterials (UWEB21). Materials support was from RTM who is an investigator of the Howard Hughes Medical Institute.

REFERENCES

[1]Acton, S., A. Rigotti, K. T. Landschulz, S. Xu, H. H. Hobbs, and M. Krieger. Identification of scavenger receptor SR-BI as a high density lipoprotein receptor. *Science* 271:518–520, 1996.

[2]Anders, H.-J., and M. Ryu. Renal microenvironments and macrophage phenotypes determine progression or resolution of renal inflammation and fibrosis. *Kidney Int*. 80:915–925, 2011.

[3]Anderson, J. M. Biological response to materials. *Annu. Rev. Mater. Res*. 31:81–110, 2001.

[4]Anderson, J. M., and J. A. Jones. Phenotypic dichotomies in the foreign body reaction. *Biomaterials* 28:5114–5120, 2007.

[5]Anderson, J. M., A. Rodriguez, and D. T. Chang. Foreign body reaction to biomaterials. *Semin. Immunol*. 20:86–100, 2008.

[6]Badylak, S. F., J. E. Valentin, A. K. Ravindra, G. P. McCabe, and A. M. Stewart-Akers. Macrophage phenotype as a determinant of biologic scaffold remodeling. *Tissue Eng. A* 14:1835–1842, 2008.

[7]Brauker, J. H., V. E. Carr-Brendel, L. A. Martinson, J. Crudele, W. D. Johnston, and R. C. Johnson. Neovascularization of synthetic membranes directed by membrane microarchitecture. *J. Biomed. Mater. Res*. 29:1517–1524, 1995.

[8]Brodbeck, W. G., G. Voskerician, N. P. Ziats, Y. Nakayama, T. Matsuda, and J. M. Anderson. In vivo leukocyte cytokine mRNA responses to biomaterials are dependent on surface chemistry. *J. Biomed. Mater. Res*. 64A:320–329, 2003.

[9]Brown, B. N., J. E. Valentin, A. M. Stewart-Akers, G. P. McCabe, and S. F. Badylak. Macrophage phenotype and remodeling outcomes in response to biologic scaffolds with and without a cellular component. *Biomaterials* 30:1482–1491, 2009.

[10]Chiu, Y.-C., M.-H. Cheng, H. Engel, S.-W. Kao, J. C. Larson, S. Gupta, and E. M. Brey. The role of pore size on vascularization and tissue remodeling in PEG hydrogels. *Biomaterials* 32:6045–6051, 2011.

[11]Duffield, J. S., S. J. Forbes, C. M. Constandinou, S. Clay, M. Partolina, S. Vuthoori, S. Wu, R. Lang, and J. P. Iredale. Selective depletion of macrophages reveals distinct, opposing roles during liver injury and repair. *J. Clin. Invest*. 115:56–65, 2005.

[12]Dunne, A., and L. A. J. O'Neill. The interleukin-1 receptor/toll-like receptor superfamily: signal transduction during inflammation and host defense. *Sci. STKE* 2003:re3, 2003.

[13]East, L., and C. M. Isacke. The mannose receptor family. *Biochim. Biophys. Acta* 1572:364–386, 2002.

[14]Gretzer, C., L. Emanuelsson, E. Liljensten, and P. Thomsen. The inflammatory cell influx and cytokines changes during transition from acute inflammation to fibrous repair around implanted materials. *J. Biomater. Sci. Polym. Ed*. 17:669–687, 2006.

[15]Hunt, J. A., B. F. Flanagan, P. J. McLaughlin, I. Strickland, and D. F. Williams. Effect of biomaterial surface charge on the inflammatory response: evaluation of cellular infiltration and TNF alpha production. *J. Biomed. Mater. Res*. 31:139–144, 1996.

[16]Jones, J. A., D. T. Chang, H. Meyerson, E. Colton, I. K. Kwon, T. Matsuda, and J. M. Anderson. Proteomic analysis and quantification of cytokines and chemokines from biomaterial surface-adherent macrophages and foreign body giant cells. *J. Biomed. Mater. Res. A* 83:585–596, 2007.

[17]Källtorp, M., S. Oblogina, S. Jacobsson, A. Karlsson, P. Tengvall, and P. Thomsen. In vivo cell recruitment, cytokine release and chemiluminescence response at gold, and thiol functionalized surfaces. *Biomaterials* 20:2123–2137, 1999.

[18]Kao, W. J., J. A. Hubbell, and J. M. Anderson. Protein-mediated macrophage adhesion and activation on biomaterials: a model for modulating cell behavior. *J. Mater. Sci. Mater. Med*. 10:601–605, 1999.

[19]Kao, W. J., and D. Lee. In vivo modulation of host response and macrophage behavior by polymer networks grafted with fibronectin-derived biomimetic oligopeptides: the role of RGD and PHSRN domains. *Biomaterials* 22:2901–2909, 2001.

[20]Kao, W. J., A. K. McNally, A. Hiltner, and J. M. Anderson. Role for interleukin-4 in foreign-body giant cell formation on a poly(etherurethane urea) in vivo. *J. Biomed. Mater. Res*. 29:1267–1275, 1995.

[21]Khramtsova, G., C. Liao, A. Khramtsov, S. Li, C. Gong, D. Huo, and R. Nanda. The M2/alternatively activated macrophage phenotype correlates with aggressive histopathologic features and poor clinical outcome in early stage breast cancer. *Cancer Res*. 69:107, 2009.

[22]Kigerl, K. A., J. C. Gensel, D. P. Ankeny, J. K. Alexander, D. J. Donnelly, and P. G. Popovich. Identification of two distinct macrophage subsets with divergent effects causing either neurotoxicity or regeneration in the injured mouse spinal cord. *J. Neurosci*. 29:13435–13444, 2009.

[23]Klosterhalfen, B., K. Junge, and U. Klinge. The lightweight and large porous mesh concept for hernia repair. *Expert Rev. Med. Devices* 2:103–117, 2005.

[24]Le, S. J., M. Gongora, B. Zhang, S. Grimmond, G. R. Campbell, J. H. Campbell, and B. E. Rolfe. Gene expression

profile of the fibrotic response in the peritoneal cavity. *Differentiation* 79:232–243, 2010.
[25]Luttikhuizen, D. T., M. C. Harmsen, and M. J. A. Van Luyn. Cellular and molecular dynamics in the foreign body reaction. *Tissue Eng*. 12:1955–1970, 2006.
[26]Luttikhuizen, D. T., M. C. Harmsen, and M. J. A. van Luyn. Cytokine and chemokine dynamics differ between rats and mice after collagen implantation. *J. Tissue Eng. Regen. Med*. 1:398–405, 2007.
[27]MacMicking, J., Q. W. Xie, and C. Nathan. Nitric oxide and macrophage function. *Annu. Rev. Immunol*. 15:323–350, 1997.
[28]Madden, L. R., D. J. Mortisen, E. M. Sussman, S. K. Dupras, J. A. Fugate, J. L. Cuy, K. D. Hauch, M. A. Laflamme, C. E. Murry, and B. D. Ratner. Proangiogenic scaffolds as functional templates for cardiac tissue engineering. *PNAS* 107:15211–15216, 2010.
[29]Malik, A. F., R. Hoque, X. Ouyang, A. Ghani, E. Hong, K. Khan, L. B. Moore, G. Ng, F. Munro, R. A. Flavell, Y. Shi, T. R. Kyriakides, and W. Z. Mehal. Inflammasome components Asc and caspase-1 mediate biomaterial-induced inflammation and foreign body response. *PNAS* 108:20095–20100, 2011.
[30]Mantovani, A., A. Sica, S. Sozzani, P. Allavena, A. Vecchi, and M. Locati. The chemokine system in diverse forms of macrophage activation and polarization. *Trends Immunol*. 25:677–686, 2004.
[31]Martinez, F. O., S. Gordon, M. Locati, and A. Mantovani. Transcriptional profiling of the human monocyte-to-macrophage differentiation and polarization: new molecules and patterns of gene expression. *J. Immunol*. 177:7303–7311, 2006.
[32]McBane, J. E., L. A. Matheson, S. Sharifpoor, J. P. Santerre, and R. S. Labow. Effect of polyurethane chemistry and protein coating on monocyte differentiation towards a wound healing phenotype macrophage. *Biomaterials* 30:5497–5504, 2009.
[33]Moilanen, E., T. Moilanen, R. Knowles, I. Charles, Y. Kadoya, N. al-Saffar, P. A. Revell, and S. Moncada. Nitric oxide synthase is expressed in human macrophages during foreign body inflammation. *Am. J. Pathol*. 150:881–887, 1997.
[34]Mokarram, N., A. Merchant, V. Mukhatyar, G. Patel, and R. V. Bellamkonda. Effect of modulating macrophage phenotype on peripheral nerve repair. *Biomaterials* 33:8793–8801, 2012.
[35]Mooney, J. E., B. E. Rolfe, G. W. Osborne, D. P. Sester, N. van Rooijen, G. R. Campbell, D. A. Hume, and J. H. Campbell. Cellular plasticity of inflammatory myeloid cells in the peritoneal foreign body response. *Am. J. Pathol*. 176:369–380, 2010.
[36]Mosser, D. M. The many faces of macrophage activation. *J. Leukoc. Biol*. 73:209–212, 2003.
[37]Murray, P. J., and T. A. Wynn. Obstacles and opportunities for understanding macrophage polarization. *J. Leukoc. Biol*. 89:557–563, 2011.
[38]Ratner, B. D. A paradigm shift: biomaterials that heal. *Polym. Int*. 56:1183–1185, 2007.
[39]Refai, A. K., M. Textor, D. M. Brunette, and J. D. Waterfield. Effect of titanium surface topography on macrophage activation and secretion of proinflammatory cytokines and chemokines. *J. Biomed. Mater. Res. A* 70A:194–205, 2004.
[40]Ricardo, S. D., H. van Goor, and A. A. Eddy. Macrophage diversity in renal injury and repair. *J. Clin. Invest*. 118:3522–3530, 2008.
[41]Rodriguez, A., H. Meyerson, and J. M. Anderson. Quantitative in vivo cytokine analysis at synthetic biomaterial implant sites. *J. Biomed. Mater. Res*. 89A:152–159, 2009.
[42]Schutte, R. J., L. Xie, B. Klitzman, and W. M. Reichert. In vivo cytokine-associated responses to biomaterials. *Biomaterials* 30:160–168, 2009.
[43]Sharkawy, A. A., B. Klitzman, G. A. Truskey, and W. M. Reichert. Engineering the tissue which encapsulates subcutaneous implants. III. Effective tissue response times. *J. Biomed. Mater. Res*. 40:598–605, 1998.
[44]Sica, A., T. Schioppa, A. Mantovani, and P. Allavena. Tumour-associated macrophages are a distinct M2 polarised population promoting tumour progression: potential targets of anti-cancer therapy. *Eur. J. Cancer* 42:717–727, 2006.
[45]Stein, M., S. Keshav, N. Harris, and S. Gordon. Interleukin 4 potently enhances murine macrophage mannose receptor activity: a marker of alternative immunologic macrophage activation. *J. Exp. Med*. 176:287–292, 1992.
[46]Tan, K. S., L. Qian, R. Rosado, P. M. Flood, and L. F. Cooper. The role of titanium surface topography on J774A.1 macrophage inflammatory cytokines and nitric oxide production. *Biomaterials* 27:5170–5177, 2006.
[47]Tang, L., and J. W. Eaton. Natural responses to unnatural materials: a molecular mechanism for foreign body reactions. *Mol. Med*. 5:351–358, 1999.
[48]Tidball, J. G., and S. A. Villalta. Regulatory interactions between muscle and the immune system during muscle regeneration. *Am. J. Physiol. Regul. Integr. Comp. Physiol*. 298:R1173–R1187, 2010.
[49]Villalta, S. A., H. X. Nguyen, B. Deng, T. Gotoh, and J. G. Tidball. Shifts in macrophage phenotypes and macrophage competition for arginine metabolism affect the severity of muscle pathology in muscular dystrophy. *Hum. Mol. Genet*. 18:482–496, 2009.
[50]Vogt, J., G. Brandes, I. Krüger, P. Behrens, I. Nolte, T. Lenarz, and M. Stieve. A comparison of different nanostructured biomaterials in subcutaneous tissue. *J. Mater. Sci. Mater. Med*. 19:2629–2636, 2008.
[51]Von Recum, A. F., and T. G. Van Kooten. The influence of micro-topography on cellular response and the implications for silicone implants. *J. Biomater. Sci. Polym. Ed*. 7:181–198, 1996.
[52]Wang, X., M. R. Lennartz, D. J. Loegering, and J. A. Stenken. Multiplexed cytokine detection of interstitial fluid collected from polymeric hollow tube implants—a feasibility study. *Cytokine* 43:15–19, 2008.
[53]Ward, W. K., E. P. Slobodzian, K. L. Tiekotter, and M. D. Wood. The effect of microgeometry, implant thickness and polyurethane chemistry on the foreign body response to subcutaneous implants. *Biomaterials* 23:4185–4192, 2002.
[54]Wynn, T. A. Cellular and molecular mechanisms of fibrosis. *J. Pathol*. 214:199–210, 2008.
[55]Xia, Z., and J. T. Triffitt. A review on macrophage responses to biomaterials. *Biomed. Mater*. 1:R1–R9, 2006.
[56]Zeyda, M., D. Farmer, J. Todoric, O. Aszmann, M. Speiser, G. Gyori, G. J. Zlabinger, and T. M. Stulnig. Human adipose tissue macrophages are of an anti-inflammatory phenotype but capable of excessive pro-inflammatory mediator production. *Int. J. Obes*. 31:1420–1428, 2007.